China Petroleum Processing and Petrochemical Technology

Catalyst Research Volume 23, Issue 2, October 2023 Pp. 2304-2319

CHEST X-RAY MULTI-CLASS DISEASES CLASSIFICATION USING DEEP LEARNING- RESNET.

K.France [a], Dr. A.Jaya[b]

[a] Research Scholar, Department of Computer Applications, B.S.Abdur Rahman Crescent Institute of Science and Technology, Chennai - 600048, India

[b] Professor, Department of Computer Applications, B.S.Abdur Rahman Crescent Institute of Science and Technology, Chennai - 600048, India.

Abstract

Chest X-ray radiography is a valuable diagnostic tool that helps doctors to identify a wide range of diseases (like Pneumonia, Lung Tumors, Pneumothorax, Tuberculosis (TB), and Enlarged Heart), affecting the chest, heart, lungs, bones, and surrounding structures. They provide detailed images of the internal structures of the chest, thus allowing doctors to visualize abnormalities and make informed diagnoses. Interpreting chest X-ray images requires specialized training and a radiologist. Even trained radiologists find it difficult to correctly diagnose disease because of the complex anatomy of the chest, overlapping structures, subtle abnormalities in the diseases, and the vast quantity of information stored in X-ray images. Radiologists need to have extensive knowledge of various diseases and their appearances to accurately diagnose them. In real-time it is very difficult to get enough specialized trained radiologists to look at all the X-ray images and generate the radiological report. There is difficulty arises when these images are interpreted by inexperienced radiologists. As a result, the healthcare sector has used machine learning and deep learning algorithms to produce automated precise radiology reports. The objective of this research paper is to classify the 14 different diseases from the given X-ray images using deep learning techniques. We implemented the Residual Neural Network (ResNet) deep learning model to classify the images, Also, we tried extended ResNet architecture (ResNet50, ResNet 101, ResNet 150) to classify the dataset images. The NIH dataset was used to classify the diseases, our dataset contains 5606 images which include 14 types of diseases. From the experimental results, the ResNet 50 architecture performs better than the other two ResNet architectures for both accuracy and ROC AUC results for training, testing, and validation datasets compete to start of art method.

Keywords: Chest X-ray, Chest Diseases, Deep Learning, ResNet, Machine Learning.

1. Introduction

The chest X-ray (CXR) is among the most commonly employed techniques in medical imaging. Radiologists rely on CXR as a fast and economical approach to detect a variety of conditions in the human body, encompassing the heart, lungs, bones, blood vessels, and air passages [1]. It has a significant role in identifying illnesses and irregularities. The creation of CXR images usually involves directing X-ray radiation through the body while it rests against the metallic surface of an X-ray device. Variations in radiation absorption by different organs lead to distinct appearances in the CXR image. Organs with higher radiation absorption (such as bones) manifest as white areas, while those with lower absorption (like the heart) exhibit various

Catalyst Research Volume 23, Issue 2, October 2023 Pp. 2304-2319

shades of gray. Air-filled structures and organs (such as the lungs and airways) are depicted as black [2]. CXR investigations are inexpensive, non-invasive, and painless. They have been recognized as a valuable tool for detecting numerous diseases and anomalies, assisting in disease diagnosis [3]. Chest disorders are dangerous if they are not recognized early. According to the World Health Organization, chest disorders have a relatively high mortality rate and can result in death in a variety of conditions. According to WHO, an estimated 65 million people worldwide suffer from COPD (chronic obstructive pulmonary disease), with 3 million deaths [4]. The mortality rate for pneumonia is concerning, as it killed 808,694 children under the age of five in 2017 [5,6]. In [7] TB infected nearly 10 million people (1.2 million children, 3.2 million women, and 5.6 million men), resulting in 1.4 million fatalities. [8] The same is true for lung cancer, which claims the lives of nearly 1.6 million individuals each year. For patient diagnosis, radiologists visually analyze CXR images. This process is resource and time-intensive, particularly in regions with a dearth of qualified medical professionals. The relatively lower image resolution of CXRs, coupled with similarities in disease indications, and the possibility of reduced focus and experience during interpretation,can present radiologists with a challenging task.These challenges may result in critical diagnostic errors that jeopardize patient well-being. As a solution, computer-aided detection systems (CAD), encompassing technologies like computer vision, machine learning (ML), and deep learning (DL) algorithms, have been proposed.

b corresponding author: jaya@crescent.education

These systems aim to serve as effective decision-making tools to aid radiologists in diagnosing various diseases [8-11]. For approximately ten years, machine learning (ML) methods gained increased prominence in the realm of anomaly detection and categorization within medical imaging.

This surge in popularity was notably fueled by the availability of diverse datasets. These ML techniques found application in multiple facets of medical image analysis, including organ segmentation and the identification and classification of diseases.

Rasheed et al [12] proved good performance in identifying numerous ailments such as tuberculosis, pneumonia, edema, cardiomegaly, and even COVID-19 after considerable research. Elaziz et al. [13] proposed a machine-learning method for differentiating between normal and COVID-19 CXR pictures. They used the fractional multichannel exponent moments (FrMEMs) technique to extract features, a modified version of manta ray foraging optimization (MRFO) to pick features, and the k-nearest neighbors (KNN) classifier to classify images. In a similar vein, Candemir et al. [13] used an algorithm with two basic stages to classify cardiomegaly in their investigation. The first part entails locating the heart and lung areas within CXR pictures, while the second phase concentrates on obtaining radiographic indices from the heart and lung borders. In their paper [14], they presented a support vector machine (SVM)--based approach for classifying atelectasis and cardiomegaly. The procedure began with segmenting CXR pictures to

locate the region of interest (ROI), followed by image enhancement using gray-level modification algorithms [15]. [16] used a mixture of five machine learning classifiers (multi-layer perceptron, decision tree, naive Bayes, support vector machine, and k-nearest neighbors). These classifiers were used with three-dimensionality reduction approaches (principal component analysis, sequential forward selection, and kernel principal component analysis) to detect instances of pediatric pneumonia. Pavithra and Pattar [17] provided a technique for recognizing and classifying CXR pictures as pneumonia or lung cancer. For noise reduction, the algorithm employs techniques like power law transformation and median filtering. A Gabor filter is used to extract features, which are then classified using both feed-forward and radial basis function methods. Furthermore, Khatri et al. used the Earth Movers Distance (EMD), a distance measurement between probability distributions. In [18], they used a variety of machine learning algorithms (Logistic Regression, Neural Network, and Support Vector Machine) to predict pneumonia occurrences in CXR pictures. A GLCM (Gray-Level Co-occurrence Matrix) technique was used to extract the features. The NIH dataset samples images of various diseases.This study investigates the different ResNet deep-learning architecture models to see which one is better for classifying the 14 types of chest ailments using chest X-ray pictures.For our implementation, we used the NIH chest X-ray picture database (images are available at https://nihcc.app.box.com/v/ChestXray-NIHCC).

2. Related work

In[19] they surveyed 223 papers using explainable artificial in- intelligence (XAI) in deep-learning-based medical image analysis, classified according to an XAI framework, and categorized according to anatomical location and imaging technique. The paper dis- cussed how to evaluate XAI, current critiques on XAI, and future perspectives for XAI in medical image analysis. [20] Building truly large-scale, fully-automated high precision medical diagnosis systems remains a strenuous task. The ChestX-ray8 dataset is often used to develop and benchmark algorithms for both weakly-supervised classification and localization of thorax diseases. Weakly-supervised learning refers to training models using images with only image-level labels rather than pixel-level annotations. This means that the model learns to classify and identify diseases in chest X-rays without knowing the exact location of the abnormalities. Each image is associated with multiple disease labels, including common thorax diseases such as pneumonia, tuberculosis, lung nodules, and more. The annotations for this dataset were generated using natural language processing (NLP) techniques to extract disease labels from associated radiology reports, resulting in weakly-supervised labels. As a result, some inaccuracies may exist in the disease labels.

Tahmina Zebinetal.[21] Used the transfer learning method to classify COVID-19 and Pneumonia from the normal image. To extract the features, they employed the VGG16, EfficientNetB0, and ResNet50 models. Among these three algorithms, EfficientNetB0 has the highest accuracy of 96.8%. In addition, the picture augmentation for COVID-19 photos was used using the generative adversarial system. The gradient class activation mapping approach is utilized for disease localization in chest X-ray images. Images, dealing with class imbalance, effective

Catalyst Research Volume 23, Issue 2, October 2023 Pp. 2304-2319

fine-tuning, and validation of the models have not been explored. [22] Proposed OXnet to detect the nine types of thoracic diseases like Aortic calcification, cardiomegaly, fracture, mass, nodule, pleural effusion, pneumonia, pneumothorax, and TB. A group of ten radiologists (4-30 years of experience) identified the lesion bounding boxes, and each picture was tagged by two with a corresponding written report. If the first radiologist differed on the annotation, the final judgment would be made by a senior radiologist (with at least 20 years of experience). [23] Proposed the VGG-based model architecture with fewer layers to detect pneumonia And used the Dynamic Histogram Enhancement technique is used to pre-process the images total of 5786 X-ray images and from the Kaggle competition the training set consisting of 4037 images separated into normal and pneumonia sub-sets,

The normal set has 1093 images, while the pneumonia set contains 2944 images. The validation set had 579 images in total, separated into normal and pneumonia sub-sets; the normal set had 157 images, while the pneumonia set had 422 images. The test set had 1170 chest images, whereas the normal and pneumonia sets contained 316 and 854 images, respectively. obtained an accuracy rating of 96.07% results.[24] Developed an algorithm that can detect pneumonia more accurately compared to practicing radiologists They used CheXNet, an architecture that has a 121-layer convolutional neural network trained on ChestX-ray14, currently the largest publicly available chest Xray dataset, containing over 100,000 frontal view X-ray images with 14 diseases. [25] The majority of prior deep neural network classifiers were designed based on deterministic, which are often extremely noise-sensitive and are prone to the overfitting problem. To overcome this issue [25] Deep generative classifiers autonomously diagnose thorax disorders from chest X-ray images. A deep generative classifier, unlike a standard deterministic classifier, features a distribution intermediate layer in the deep neural network. The distribution layer is then sampled at random by a sampling layer, which is then classified by the next layer. Because the class label is created from samples of a related distribution, the classifier is generative. Deep generative classifiers are anticipated to be resilient to noise, avoid overfitting, and achieve high performance by training the model with a given level of randomness. Our deep generative classifiers were built using a variety of well-known deterministic neural network designs.

Ha Min Sonet al. [26] Most of the existing computer-aided diagnosis (CAD) systems are focused on improving the quality of mammography and colonography there is not much work done in dermatology, in this work, they have proposed a segmentation technique using U-Net to classify the various skin diseases. [27] This research examines a Deep Convolutional Neural Network U-Net architecture-based end-to-end strategy for identifying Cardiomegaly disease. The open-source medical dataset "ChestX-ray8" was utilized. The Adaptive Histogram Equalization (AHE) method is used to increase the contrast and brightness of the original database. Using this method, they achieved a diagnostic image accuracy of higher than 93%. Furthermore, U-Net can pinpoint the specific location of Cardiomegaly. [28] The research used deep CNN models to identify lung abnormalities and diagnose particular TB symptoms in seven TB-related lung disorders (consolidation, effusion, fibrosis, infiltration, mass, nodule, and pleural thickening). Various training/validation methods.

Catalyst Research Volume 23, Issue 2, October 2023 Pp. 2304-2319

[29] The study focuses on pneumonia identification as an example of a disease that may be recognized and treated early to prevent subsequent problems. Several deep learning models are highlighted, including LeNet, AlexNet, ZFNet, VGG-16/19, and GoogLeNet, as well as their contributions to the discipline. Overall, the document underlines the need to apply deep learning techniques to automate the X-ray diagnosis process to enhance healthcare services, particularly in places with limited access to radiologists.The proposed method is less invasive than pricey scans and gives a simpler and more affordable solution for Parkinson's disease screening. The paper also highlights the work's key achievements, such as the non-invasive technique, improved pipelines, compact model, performance assessment comparison, and implementation in sophisticated gadgets [30].To highlight the benefits of technological change in healthcare, it finishes with predictions about the direction of healthcare technology and case examples from Poland and Africa. In general, the document offers insightful information about the digital revolution of the healthcare sector and its potential influence on enhancing the quality of healthcare and products [31].

Due to the minor changes in the chest X-ray, finding appropriate deep-learning techniques to classify chest diseases is a challenging task. Additionally, dependent on the deep learning architecture and the hyperparameters that are utilized in the specific deep learning model, the disease prediction accuracy rate will change.This study investigates the different ResNet deep-learning architecture models to see which one is better for classifying the 14 types of chest ailments using the NIH chest X-ray image dataset.The background information and research-related works on deep learning-based chest illness detection and classification are presented in Section 2.Section 3 provides more information on the materials and techniques, the dataset used for the study, data preparation, and the suggested deep learning architecture.Section 4 integrates the findings, together with experimental settings, performance measures, and comparisons to existing cutting-edge systems for the detection and categorization of chest disorders.Finally, Section 5 provides findings and potential directions for further future investigation.

3. Proposed Method

Previous studies on the ChestX-ray14 dataset have mainly focused on the architectural models ResNet-50 and DenseNet-121. The ResNet-50 architecture is the subject of our experimental interest due to its outstanding performance in the area of computer vision [32]. To modify the initial architecture and tailor the network to our specific objective, we add a sigmoid activation function to address our multi-label problem and replace the last dense layer with a new dense layer that matches the number of labels (details can be found in Table 1).

Catalyst Research Volume 23, Issue 2, October 2023 Pp. 2304-2319

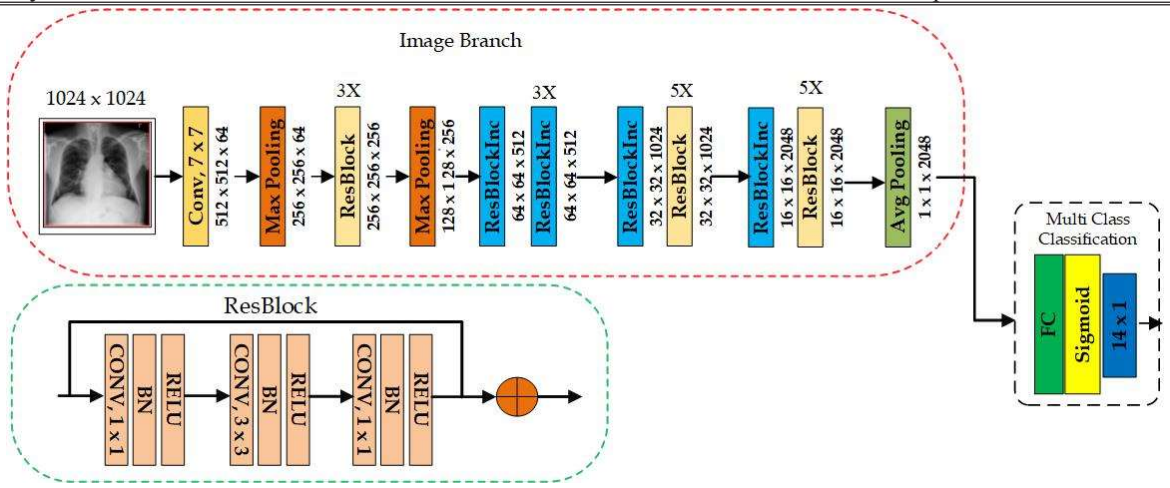

Figure 1. Architecture diagram of modified ResNet 50 Model: Our design is built on top of the R esNet-50 model. After the first three ResBlocks, we added a max-polling layer because the input size had grown.

3.1 Architectures

We use two variations of the ResNet-50 architecture in addition to the original: To begin, we restrict the number of input channels to one (the ResNet-50 is meant to handle RGB images from the ImageNet dataset), which should make training an X-ray-specific CNN easier. Second, we multiply the input size by two (i.e. 1024 x 1024). We only add a new max-pooling layer after the first bottleneck block to keep the model architectures consistent. The parameters of this max-pooling layer are the same as those of the "pooling1" layer (i.e. 3 3 kernel, stride 2, and padding). Our alterations are depicted in the image branch of Figure 1. A better effective resolution may be advantageous for detecting small structures that may be symptomatic of pathology (for example, masses and nodules). Finally, we investigate various model depths using the best-performing configuration (ResNet50, ResNet101, ResNet152).

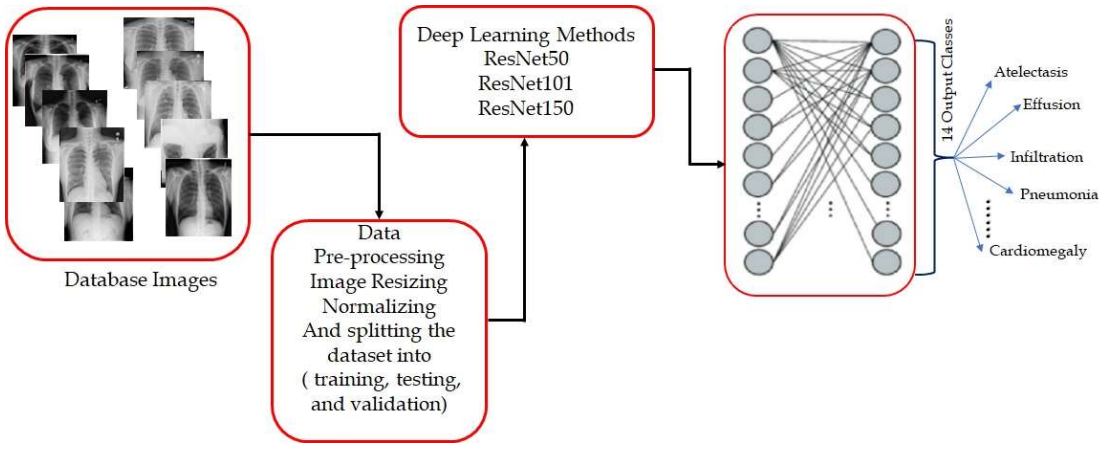

Figure 2. Workflow diagram of the proposed method.

In a block diagram, Figure 2. shows the suggested framework. It involves three steps data pre-processing, feature extraction using ResNet deep learning models, and disease classification. During the first steps, the input X-ray images are preprocessed with functions such as

normalization, scaling, and cropping. Then input images are split into training, testing, and validation datasets. In the second step features are extracted from the images using a deep-learning model ResNet50, ResNet101, and ResNet152. The third step fully connected layer is used to categorize all 14 types of diseases.

Table 1: The original architecture and our off-the-shelf and fine-tuned ResNet-50 differ in several aspects. The changes we made to our application are highlighted. Unlike the original network, all layers in our architecture employ automatic padding to maintain the spatial size. Additionally, the conv3_0, conv4_0, and conv5_0 layers in our architecture down-sample the spatial size with a stride of 2.

Layername	Outputsize	OriginalSO-layer	Off-the-shelf	Fine-tuned
convl	112x112	7x7,64-d,stride2	same	fine-tuned
poolingl	56x56	3x3,64-d,maxpool,stride2	same	same
conv2_x	56x56	[1x1,64-d,stride 1 3x3,64-d,stride 1 1x 1,256-d, stride 1] x 3	same	fine-tuned
conv3_0	28x28	[1 x 1, 128-d, stride2 3 x 3, 128-d, stridel 1 x 1, 512-d, stridel]	same	fine-tuned
conv3_x	28x28	[1x1,128-d,stridel 3x3,128-d,stridel 1x1,512-d,stridel] x 3	same	fine-tuned
conv4_0	14x14	[1x1,256-d,stride2 3x3,256-d,stridel 1x 1,1024-d,stridel]	same	fine-tuned
conv4_x	14x14	[1x 1,256-d,stridel 3x3,256-d,stridel 1x 1,1024-d,stridel] x 5	same	fine-tuned
conv5_0	7x7	[1x 1,512-d,stride2 3x3,512-d,stridel 1x 1,2048-d,stridel]	same	fine-tuned

conv5_x	7x7	[1x 1,512-d,stride1 3x3,512-d,stride1 1x 1,2048-d,stride1] x 2	same	fine-tuned
pooling2	1x1	7x7,2048-d,averagepool, stride1	same	fine-tuned
dense	1x1	1000-d,dense-layer	14-d,dense-layer	
loss	1x1	1000-d,softmax	14-d,sigmoid	

3.2 Dataset

The NIH Chest X-ray image Dataset consists of 112,120 X-ray images, they are classified into 14 types of diseases based on the radiologist's reports from 30,805 unique patients [31]. For our implementation purpose, we have used the randomly sampled Kaggle dataset (https://www.kaggle.com/datasets/nih-chest-xrays/sample)which contains 5606 images which include all 14 types of diseases, see the sample images from the database in Figure 3. The statistics of chest X-ray images included in this study are shown in Table 2. We divided the dataset (4000, 1003, 603) into train, test, and validation sets randomly.

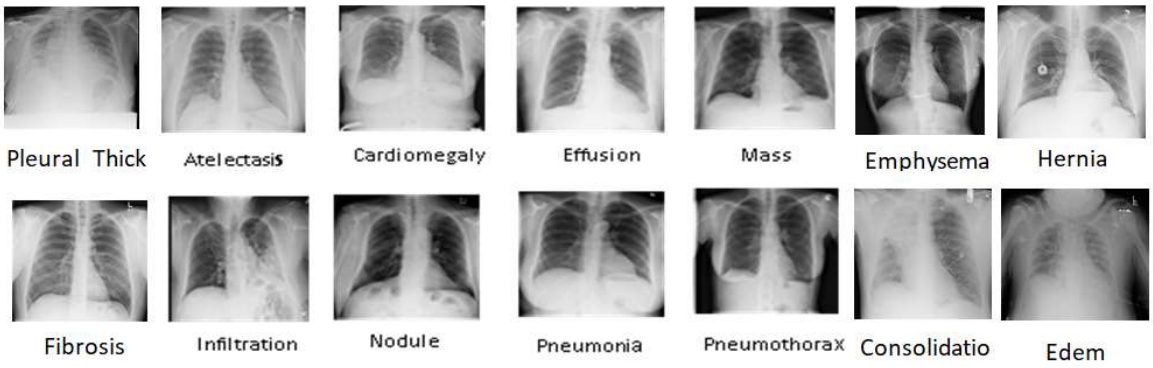

Figure 3. Sample images from the NIH dataset

Table 2: Statistics of chest X-ray images

Si.NO	Diseases	No. of Images
1	Atelectasis	507
2	Cardiomegaly	126
3	Consolidation	161
4	Edema	94
5	Effusion	383
6	Emphysema	84
7	Fibrosis	57
8	Hernia	7
9	Infiltration	640

Catalyst Research Volume 23, Issue 2, October 2023 Pp. 2304-2319

10	Mass	148
11	Nodule	158
12	Pleural_Thickening	72
13	Pneumonia	14
14	Pneumothorax	111
15	No findings	3044
	Total	**5606**

4. Experiments and Results

We used our laptop for the implementation with a configuration of i7 (7th Generation) processor, 16GBRAM,4GB NVIDIA graphs card, used Python version 3.10.9 with PyTorch 2.0.1 software and Jupyter Notebook editor, along with necessary data analysis library like pandas, numpy, scipy, etc. The ADAM optimizer was used and the learning rate = 0.0001, RELU activation function, batch size = 128, and epochs =30 were used during the implementation.

Results The overall training accuracy of the dataset is shown in Table 3. The outcome shows that, exceptfor the effusion, all diseases perform better with the ResNet 50 model. Also, we observed that the ResNet101 model was overfitting during the training dataset. The ROC AUC score (receiver operating characteristic curve) was calculated for the training, testing, and validation dataset. The results are mentioned in Table 4, It shows that ResNet50 architecture gives better results than ResNet 101 and ResNet 152. Figure 4, Figure 5, and Figure 6 represent the ROC AUC curve representation of training, testing, and validation datasets. The highest accuracy and AUC ROC of about 98% results were obtained for Herina disease which has very few positive samples in the dataset. The ResNet50 architecture model gave the better AUC ROC for most of the diseases. Although our suggested network architecture achieves remarkable AUC values for all categories of the ChestX-ray14 dataset, the clinical applicability of such technology is primarily dependent on the availability of data for both training and testing the model.We are already getting positive results for the different ResNet models. We have specifically observed improved performance for minor diseases like nodules and masses. We have seen equivalent or somewhat lower performance levels for other disorders, though.Compare our results with Wang et al. our proposed model gives the highest results for 7 diseases it shows in Table 5.

There was no official dataset separation, and just the pictures from ChestX-ray14 were made available to the public. Scientists began creating their data divisions for training and testing as a result. Based on the resampling there were observable performance differences. A direct comparison to the results of other research findings may be misleading when attempting to evaluate state-of-the-art performance.The accuracy and ROC value were calculated using equations 1, 2, and 3

$$\text{Accuracy} = \frac{TP+TN}{TP+FP+TN+FN} \quad (1)$$

ROC curve

True Positive Rate (TPR)

$$TPR = \frac{TP}{TP+F} \quad (2)$$

False Positive Rate (FPR)

$$FPR = \frac{FP}{FP+TN} \quad (3)$$

Were

TP- True Positive (Positive Classes That are correctly predicted as positive)

TN- True Negatives (Negative Classes That are correctly predicted as negative)

FP- False Positives (Negative Classes That are Falsely Predicted as positeve)

FN- False Negatives (Positive Classes That are falsely Predicted as Negative

Table 3: Accuracy result of our experiments during the training, testing, and validation dataset. The bold text highlighted the overall highest accuracy among the three ResNet models.

Train Dataset Accuracy Report					Test Dataset Accuracy Report			Validation Dataset Accuracy Report		
Labels		ResNet 50	ResNet 101	ResNet 152	ResNet 50	ResNet 101	ResNet 152	ResNet 50	ResNet 101	ResNet 152
0	Cardiomegaly	**79.95**	70.975	61.05	77.666999	69.99003	61.814556	77.777778	72.139303	57.21393
1	Emphysema	**81.9**	68.1	72.875	81.05683	64.107677	70.588235	81.094527	64.344942	69.651741
2	Effusion	67.95	78.95	64.55	67.298106	78.963111	60.717846	69.485904	78.441128	59.701493
3	Hernia	**98.9**	71.575	96.45	98.005982	69.790628	96.011964	98.839138	71.641791	97.512438
4	Nodule	**82.025**	44.875	70.6	79.262213	46.161515	68.394816	75.953566	46.434494	68.490879
5	Pneumothorax	**79.35**	0	70.3	76.66999	0	69.890329	79.104478	0	66.998342
6	Atelectasis	73.5	0	57.45	71.385842	0	55.832502	69.983416	0	53.565506
7	Pleural_Thickening	76.175	0	69.65	73.978066	0	66.201396	71.641791	0	67.661692
8	Mass	77.45	0	68.525	73.678963	0	66.500499	73.631841	0	66.334992
9	Edema	81.775	0	69.775	80.259222	0	69.690927	83.747927	0	65.505804
10	Consolidation	76.15	0	74.8	73.778664	0	73.579262	74.461028	0	72.139303
11	Infiltration	68.25	0	64.95	63.010967	0	64.307079	63.349917	0	60.364842
12	Fibrosis	**84.7**	0	77.275	82.751745	0	76.370887	83.913765	0	73.963516
13	Pneumonia	**84.35**	0	66.675	84.546361	0	68.594217	85.903814	0	65.671642

Table 4: The ROC AUC score (receiver operating characteristic curve) for training, testing, and validation dataset

	Train Dataset ROC AUC Score				Test Dataset ROC AUC Score			Valication Dataset ROC AUC Score		
Labels		ResNet 50	ResNet 101	ResNet 152	ResNet50	ResNet101	ResNet152	ResNet50	ResNet101	ResNet152
0	Cardiomegaly	**0.919306**	0.500738	0.789666	0.500738	0.480738	0.707531	**0.824317**	0.72531	0.781973
1	Emphysema	**0.944472**	0.705766	0.824107	**0.705766**	0.685766	0.814879	**0.813846**	0.765892	0.734354
2	Effusion	**0.826478**	0.757312	0.76627	**0.757312**	0.706312	0.749508	0.726846	0.734321	0.721817
3	Hernia	**0.999937**	0.8002	0.996837	**0.8002**	0.8002	0.672422	**0.85624**	0.77543	0.847176
4	Nodule	**0.833258**	0.525952	0.712367	0.525952	0.525952	0.631436	**0.964523**	0.63529	0.563372
5	Pneumothorax	0.89207	0	0.799088	**0.778865**	0.763565	0.745695	**0.85935**	0.728342	0.755516
6	Atelectasis	0.819509	0	0.725742	**0.710225**	0.680225	0.678811	**0.718236**	0.765429	0.663946
7	Pleural_Thickening	0.901213	0	0.79241	0.691978	0.631978	0.62349	**0.77466**	0.753694	0.701566
8	Mass	0.849667	0	0.717505	0.643536	0.603536	0.616122	0.692432	0.593573	0.638337
9	Edema	0.953068	0	0.850742	**0.780599**	0.730599	0.82735	**0.738505**	0.76548	0.785593
10	Consolidation	0.885701	0	0.800321	**0.720424**	0.704243	0.729517	**0.838321**	0.68459	0.739435
11	Infiltration	0.755792	0	0.68319	0.64173	0.601731	0.621881	**0.745733**	0.664387	0.596094
12	Fibrosis	0.963384	0	0.858273	0.4805	0.432543	0.719191	0.654549	0.59834	0.539635
13	Pneumonia	0.97035	0	0.78788	0.57288	0.56568	0.695106	**0.757312**	0.72539	0.691275

Table 5: Results for our top-performing design at various depths are shown in the table below. The highest AUC value overall is shown in bold letters.

ROC AUC Score			
Labels	**Pathology**		**Proposed Architecture**

Catalyst Research Volume 23, Issue 2, October 2023 Pp. 2304-2319

		Wang et al [29]	ResNet50	ResNet101	ResNet152
0	Cardiomegaly	0.81	**0.824317**	0.72531	0.781973
1	Emphysema	0.833	0.813846	0.765892	0.734354
2	Effusion	0.759	0.726846	0.734321	0.721817
3	Hernia	0.872	0.85624	0.77543	0.847176
4	Nodule	0.669	**0.964523**	0.63529	0.563372
5	Pneumothorax	0.799	**0.85935**	0.728342	0.755516
6	Atelectasis	0.7	0.718236	0.765429	0.663946
7	Pleural_Thickening	0.684	**0.77466**	0.753694	0.701566
8	Mass	0.693	0.692432	0.593573	0.638337
9	Edema	0.805	0.738505	0.76548	0.785593
10	Consolidation	0.703	**0.838321**	0.68459	0.739435
11	Infiltration	0.661	**0.745733**	0.664387	0.596094
12	Fibrosis	0.786	0.654549	0.59834	0.539635
13	Pneumonia	0.658	**0.757312**	0.72539	0.691275

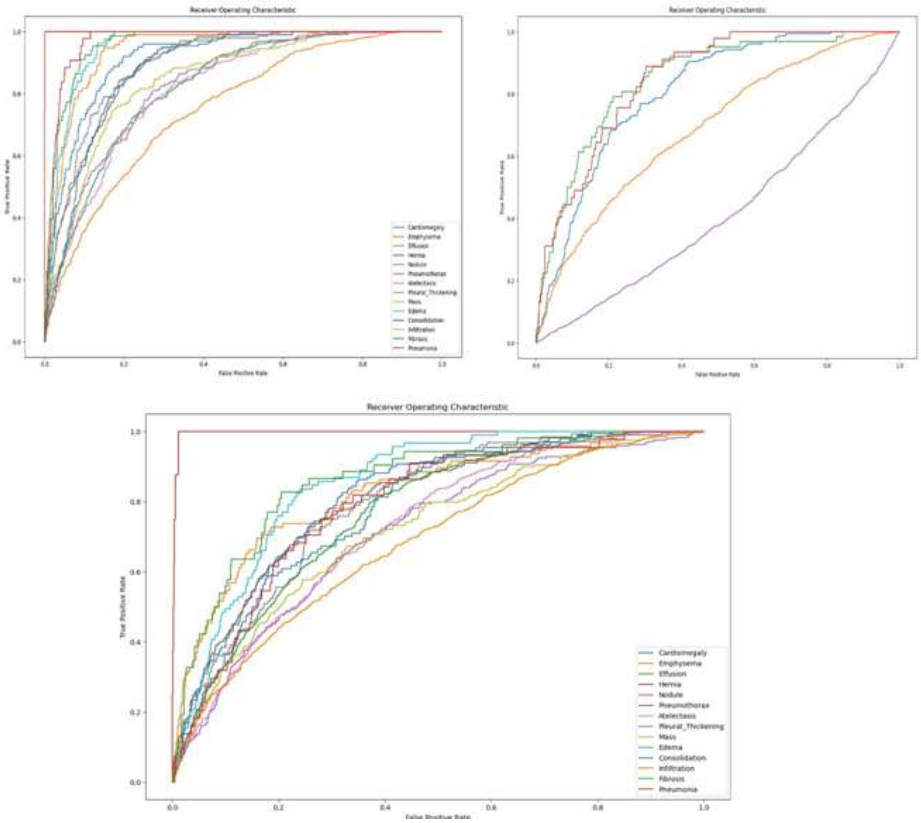

Figure 4. ROC AUC curve for Training image dataset ResNet50, ResNet101, ResNet 152

Catalyst Research Volume 23, Issue 2, October 2023 Pp. 2304-2319

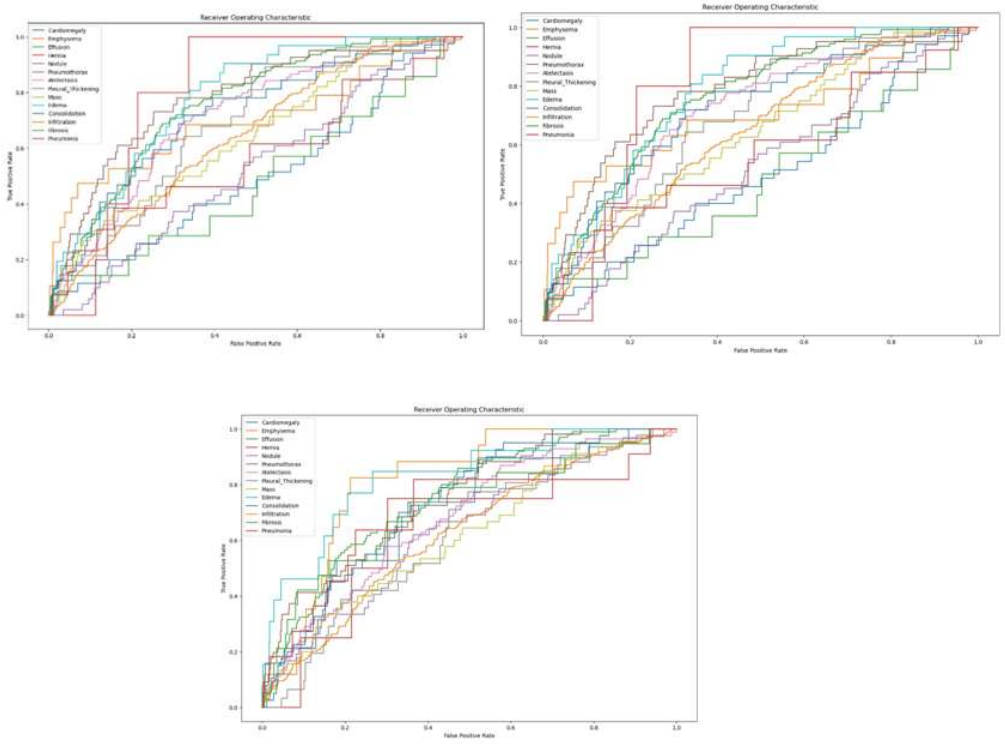

Figure 5. ROC AUC curve for Testing image dataset ResNet50, ResNet101, ResNet 152

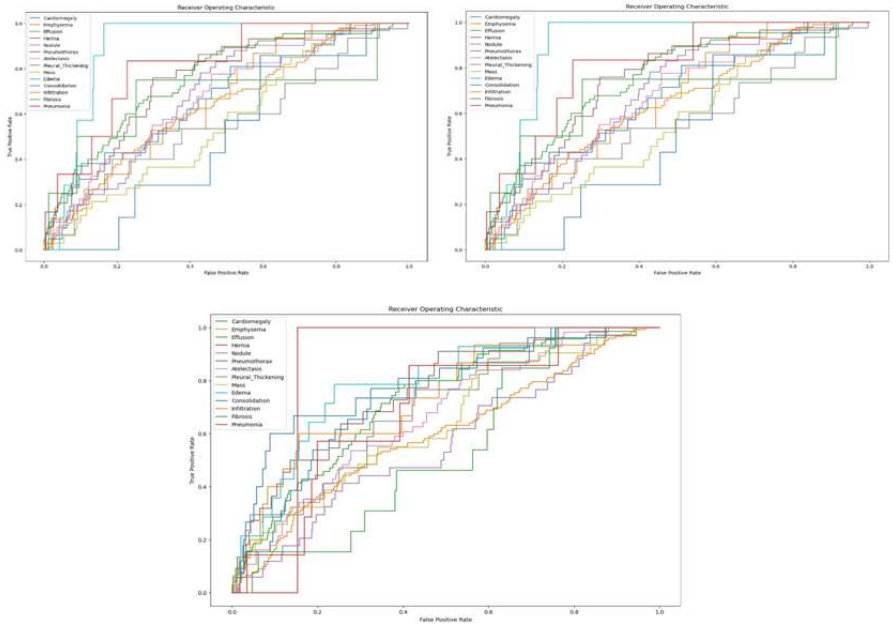

Figure 6. ROC AUC curve for Validation image dataset ResNet50, ResNet101, ResNet 152

5. Conclusion

This research work explores the ResNet-based deep learning architectures (ResNet50, ResNet101, ResNet152) to classify the 14 types of common thoracic diseases such as Atelectasis, Cardiomegaly, Consolidation, Edema, Effusion, Emphysema, Fibrosis, Hernia, infiltration, Mass,

Catalyst Research Volume 23, Issue 2, October 2023 Pp. 2304-2319

Nodule, Pleural_Thickening, Pneumonia, Pneumothorax, No findings. ResNet50 pre-trained model gave the best accuracy performance for the test, training, and validation dataset it gives an overall accuracy of 73%. Also, the ResNet50 achieved an ROC of 89% in the training dataset, and 66% in the test dataset. After analyzing our results, it was clear that the ResNet101 model had overfitted during the training phases. It performs only detecting the five diseases. We assume that the reason for overfitting occurs because of the lack of training dataset. Particularly in the context of certain diseases, this method is inadequate at efficiently managing variability within the dataset. Also, the ResNet50 model successfully detects other diseases like Cardiomegaly, Emphysema, hernia, Nodule, Pneumothorax, Edema, Fibrosis, and Pneumonia with more than 80% of training accuracy.Our optimizationwhen comparing the AUC ROC ResNet50 deep learning architecture achieves state-of-the-art results in 7 out of fourteen classes compared to Wang et al.[29] In future work, we will add more training images to avoid the overfitting issue, Also we can use some preprocessing methods to get a more accurate result in the maximum number of diseases and implementation of different CNN architectures to get the better performance.

References

1. Abiyev, R.; Ma'aitah, M.K.S. Deep Convolutional Neural Networks for Chest Diseases Detection. J. Healthc. Eng. 2018, 2018, 4168538. [CrossRef] [PubMed]
2. Radiological Society of North America. X-ray Radiography-Chest. Available online: https://www.radiologyinfo.org/en/info. cfm?pg=chestrad (accessed on 1 November 2022).
3. US Food and Drugs Administration. Medical X-ray Imaging. Available online: https://www.fda.gov/radiation-emittingproducts/ medical-imaging/medical-x-ray-imaging (accessed on 1 November 2022).
4. Marciniuk, D.; Schraufnagel, D.; Society, E.R. The Global Impact of Respiratory Disease; European Respiratory Society: Lausanne, Switzerland, 2017.
5. World Health Organization. Pneumonia Dashboard. Available online: https://www.who.int/news-room/fact-sheets/detail/pneumonia (accessed on 1 November 2022).
6. Khoiriyah, S.A.; Basofi, A.; Fariza, A. Convolutional Neural Network for Automatic Pneumonia Detection in Chest Radiography. In Proceedings of the International Electronics Symposium (IES), Surabaya, Indonesia, 29–30 September 2020; pp. 476–480.
7. World Health Organization. Tuberculosis. Available online: https://www.who.int/news-room/fact-sheets/detail/tuberculosis (accessed on 1 November 2022).
8. Sathitratanacheewin, S.; Sunanta, P.; Pongpirul, K. Deep learning for automated classification of tuberculosis-related chest X-ray: Dataset distribution shift limits diagnostic performance generalizability. J. Am. Med. Inform. Assoc. 2020, 6, 593–604. [CrossRef] [PubMed]
9. Avni, U.; Greenspan, H.; Konen, E.; Sharon, M.; Goldberger, J. X-ray Categorization and Retrieval on the Organ and Pathology Level, Using Patch-Based Visual Words. IEEE Trans. Med. Imaging 2011, 30, 733–746. [CrossRef]

10. Jaeger, S.; Karargyris, A.; Candemir, S.; Folio, L.; Siegelman, J.; Callaghan, F.; Xue, Z.; Palaniappan, K.; Singh, R.; Antani, S.; et al. Automatic Tuberculosis Screening Using Chest Radiographs. IEEE Trans. Med. Imaging 2014, 33, 233–245. [CrossRef] [PubMed]
11. Pattrapisetwong, P.; Chiracharit, W. Automatic lung segmentation in chest radiographs using shadow filter and multilevel thresholding. In Proceedings of the International Computer Science and Engineering Conference (ICSEC), Chiang Mai, Thailand, 14–17 December 2016; pp. 1–6.
12. Rasheed, J.; Hameed, A.A.; Djeddi, C.; Jamil, A.; Al-Turjman, F. A machine learning-based framework for diagnosis of COVID-19 from chest X-ray images. Interdiscip. Sci. Comput. Life Sci. 2021, 13, 103–117. [CrossRef]
13. Elaziz, M.A.; Hosny, K.M.; Salah, A.; Darwish, M.M.; Lu, S.; Sahlol, A.T. New machine learning method for image-based diagnosis of COVID-19. PLoS ONE 2020, 15, e0235187. [CrossRef]
14. Candemir, S.; Jaeger, S.; Lin, W.; Xue, Z.; Antani, S.; Thoma, G. Automatic heart localization and radiographic index computation in chest X-rays. In Medical Imaging 2016: Computer-Aided Diagnosis 2016; SPIE: Bellingham, WA, USA, 2016; pp. 302–309.
15. Alslatie, M.; Alquran, H.; Mustafa, W.A.; Abu-Qasmieh, I.; Alqudah, A.M.; Alkhayyat, A. Automated Diagnosis of Heart- Lung Diseases in Chest X-ray Images. In Proceedings of the 5th International Conference on Engineering Technology and its Applications (IICETA), Al-Najaf, Iraq, 31 May–1 June 2022; pp. 537–541.
16. Sousa, R.; Marques, O.; Curado, G.; da Costa, R.; Soares, A.; Soares, F.A.; de Oliveira, L. Evaluation of Classifiers to a Childhood Pneumonia Computer-Aided Diagnosis System. In Proceedings of the 27th International Symposium on Computer-Based Medical Systems, New York, NY, USA, 27–29 May 2014; pp. 477–478.
17. Pavithra, R.; Pattar, S. Detection and classification of lung disease-pneumonia and lung cancer in chest radiology using artificial neural network. Int. J. Sci. Res. Publ. 2015, 5, 128–132.
18. Das, S.; Kumar Pradhan, S.; Mishra, S.; Pradhan, S.; Pattnaik, P.K. A Machine Learning based Approach for Detection of Pneumonia by Analyzing Chest X-ray Images. In Proceedings of the 9th International Conference on Computing for Sustainable Global Development (INDIACom), New Delhi, India, 23–25 March 2022; pp. 177–183.
19. Bas H.M. van der Velden , Hugo J. Kuijf, Kenneth G.A. Gilhuijs, Max A. Viergever : Explainable artificial intelligence (XAI) in deep learning-based medical image analysis PP 1-21 May 2022 https://doi.org/10.1016/j.media.2022.102470
20. Xiaosong Wang, Yifan Peng, ChestX-ray8: Hospital-scale Chest X-ray Database and Benchmarks on Weakly-Supervised
Classification and Localization of Common Thorax Diseases, IEEE Conference on Computer Vision and Pattern Recognition(2017).
21. Tahmina Zebin, ShahadateRezvy COVID-19 detection and disease progression visualization: Deep learning on chest X-rays for

Classification and coarse localization, Applied Intelligence (2021) 51:1010–1021, https://doi.org/10.1007/s10489-020-01867-1.
22. Luyang Luo, Hao Chen, Yanning Zhou, Huangjing Lin, and Pheng-Ann Heng: OXnet: Deep Omni-supervised Thoracic Disease
Detection from Chest X-rays, arXiv:2104.03218v2 [cs.CV] 8 Jul 2021
23. Dejun Zhang , Fuquan Ren , Yushuang Li, Lei Na and Yue Ma: Pneumonia Detection from Chest X-ray Images Based on
Convolutional Neural Network, Electronics 2021, 10, 1512. https://doi.org/10.3390/electronics10131512
24. Pranav Rajpurkar, Jeremy Irvin, Kaylie Zhu 1 Brandon Yang, CheXNet: Radiologist-Level Pneumonia Detection on Chest X-
Rays with Deep Learning arXiv:1711.05225v3 [cs.CV] 25 Dec 2017
25. Chengsheng Mao, Yiheng Pan, Zexian Zeng, Liang Yao, Yuan Luo, Deep Generative Classifiers for Thoracic Disease Diagnosis
with Chest X-ray Images.
26. Ha Min Son, Wooho Jeon, Jinhyun Kim, Chan Yeong Heo, Hye Jin Yoon, Ji-Ung Park ,Tai-Myoung Chung , AI-based localization
and classification of skin disease with erythema, Scientific Reports, (2021) https://doi.org/10.1038/s41598-021-84593-z.
27. Bouslama , Yassin Laaziz, Abdelhak Tali, Diagnosis and precise localization of cardiomegaly disease using U-NET, Informatics
in Medicine Unlocked (2020), https://doi.org/10.1016/j.imu.2020.100306.
28. Ruihua Guo, Kalpdrum Passi, and Chakresh Kumar Jain, Tuberculosis Diagnostics and Localization in Chest X-Rays via Deep
Learning Models, Frontiers in Artificial Intelligence , October 2020, Volume 3, doi: 10.3389/frai.2020.583427.
29. Tapan Kumar Das, et al. “Chest X-Ray Investigation: A Convolutional Neural Network Approach.” Journal of Biomimetics, Biomaterials and Biomedical Engineering, vol. 45, no. 10.4028/www.scientific.net/JBBBE.45.57, 1 May 2020, pp. 57–70, https://doi.org/10.4028/www.scientific.net/jbbbe.45.57
30. Chiranji Lal Chowdhary, and R. Srivatsan. “Non-Invasive Detection of Parkinson’s Disease Using Deep Learning.” International Journal of Image, Graphics and Signal Processing, vol. 14, no. 2, 8 Apr. 2022, pp. 38–46, https://doi.org/10.5815/ijigsp.2022.02.04.
31. Channi, Harpreet Kaur, et al. “Digital Transformation in Healthcare Industry: A Survey.” Next Generation Healthcare Informatics, 2022, pp. 279–293, https://doi.org/10.1007/978-981-19-2416-3_16.
32. Xiaosong Wang, Yifan Peng, Le Lu, Zhiyong Lu, Mohammad Hadi, Ronald M. Summers, ChestX-ray8: Hospital-scale Chest X-

Catalyst Research Volume 23, Issue 2, October 2023 Pp. 2304-2319

33. X-ray Database and Benchmarks on Weakly-Supervised Classification and Localization of Common Thorax Diseases, IEEE CVPR 2017, pp. 2097-2106 (2017),https://doi.org/10.1109/CVPR.2017.369